Toward Optimized VR/AR Ergonomics: Modeling and Predicting User Neck Muscle Contraction

Yunxiang Zhang, Kenneth Chen, Qi Sun
New York University, USA
{yunxiang.zhang,kennychen,qisun}@nyu.edu

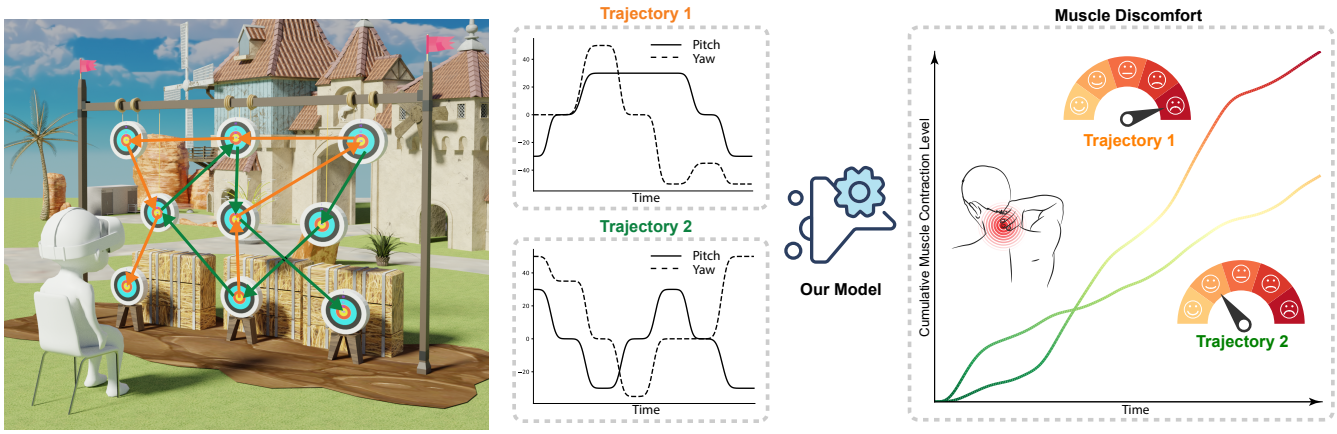

(a) two head motion trajectories in VR

(b) model-predicted cumulative neck muscle contraction and discomfort levels over time

Figure 1: ***Predicting the neck muscle contraction and discomfort levels of VR users.*** **(a) A VR user chooses between two candidate head motion trajectories of seemingly similar muscular workload for a visual task. (b) Our computational model predicts the user's potential neck muscle contraction level and thus perceived neck muscle discomfort before the movements happen. 3D asset credits to Mixall, Bizulka, RootMotion at Unity, and shockwavegamez01, joseVG at Sketchfab.**

ABSTRACT

Ergonomic efficiency is essential to the mass and prolonged adoption of VR/AR experiences. While VR/AR head-mounted displays unlock users' natural wide-range head movements during viewing, their neck muscle comfort is inevitably compromised by the added hardware weight. Unfortunately, little quantitative knowledge for understanding and addressing such an issue is available so far.

Leveraging electromyography devices, we measure, model, and predict VR users' neck muscle contraction levels (MCL) while they move their heads to interact with the virtual environment. Specifically, by learning from collected physiological data, we develop a bio-physically inspired computational model to predict neck MCL under diverse head kinematic states. Beyond quantifying the cumulative MCL of completed head movements, our model can also predict potential MCL requirements with target head poses only. A series of objective evaluations and user studies demonstrate its prediction accuracy and generality, as well as its ability in reducing users' neck discomfort by optimizing the layout of visual targets. We hope this research will motivate new ergonomic-centered designs for VR/AR and interactive graphics applications. Source code is released at: https://github.com/NYU-ICL/xr-ergonomics-neck-comfort.

SIGGRAPH '23 Conference Proceedings, August 6–10, 2023, Los Angeles, CA, USA

ACM ISBN 979-8-4007-0159-7/23/08…$15.00
https://doi.org/10.1145/3588432.3591495

CCS CONCEPTS

• **Computing methodologies** → **Virtual reality**; **Mixed / augmented reality**; **Neural networks**; • **Human-centered computing** → **Human computer interaction (HCI)**.

KEYWORDS

Ergonomics, Electromyography, Head-Mounted Display

ACM Reference Format:
Yunxiang Zhang, Kenneth Chen, Qi Sun. 2023. Toward Optimized VR/AR Ergonomics: Modeling and Predicting User Neck Muscle Contraction. In *Special Interest Group on Computer Graphics and Interactive Techniques Conference Conference Proceedings (SIGGRAPH '23 Conference Proceedings), August 6–10, 2023, Los Angeles, CA, USA.* ACM, New York, NY, USA, 13 pages. https://doi.org/10.1145/3588432.3591495

1 INTRODUCTION

VR/AR devices unlock natural viewing experiences via their uniquely wide-field displays. With head tracking, users can move their heads to shift attention and interact with peripheral content [Bahill et al. 1975; Monteiro et al. 2021]. However, their current head-mounted form factors incur non-trivial "in vitro" weight and shift the head's

natural center of mass [Chen et al. 2021]. The resulting changes in neck muscle state and workload have been evidenced to cause discomfort and injuries [Chihara and Seo 2018; Forde et al. 2011; Marklin Jr et al. 2022; Penumudi et al. 2020; Souchet et al. 2022]. Despite emerging evidence and concerns over such ergonomic side effects, comprehensively assessing and optimizing VR users' muscular comfort is still in its infancy.

A major cause of ergonomic discomfort is muscle fatigue and stress [Lowe 1996], especially from external weights, e.g., HMDs [Chihara and Seo 2018; Knight and Baber 2004]. Unlike optically trackable body movements, measuring muscular activities is remarkably difficult. Besides indirect sensing such as calorimetry [Holdy 2004], biometrics from electromyography (EMG) sensors reveal muscular status via its detected electric potential generated by muscle fibers. In fact, the EMG signals directly correlate to muscle contraction [Komi and Viitasalo 1976]. Therefore, extensive literature attempted to understand our muscular functionalities during daily tasks, with face/gaze [Manssuer et al. 2016], arm/hand [Zhang et al. 2022], and full-body [Brown et al. 2021].

Recent attention has arisen to measure the influence of emerging usage of HMDs [Chen et al. 2021]. For instance, Chihara et al. [2018] measured and associated the altered muscular contraction with ergonomic discomfort by studying various viewing and interaction postures. However, surprisingly, we still have little quantitative knowledge of the introduced ergonomic effects before deploying a VR/AR application. Computationally forecasting muscle contraction is the foundation toward the ultimate aim - systematically optimizing visual content for ergonomically enhanced VR/AR.

We present a biophysically-inspired model to predict VR users' neck muscular contraction and thus potential ergonomic discomforts over time. The model is applicable to both after (given a head trajectory) and before (given a target position) users' head movements. We first perform a physiological study in VR to obtain EMG-sensed biometrics from characterized natural head movements. The analysis reveals muscle contraction's significant correlations with head poses and motion patterns. Developed upon the data, our biophysical model first predicts the instantaneous muscle contraction given a head pose and angular acceleration. Then, by approximating representative trajectories [Farshadmanesh et al. 2012], the model further extends to forecast potential discomfort given only the target location and before the head movement occurs.

Our objective measurements and user studies demonstrate the model's: 1) prediction accuracy and generalizability with both post-hoc estimation and pre-hoc prediction, 2) capability in optimizing visual target layouts to reduce user-perceived muscular discomfort.

We hope this research will motivate new ergonomic-centered designs for VR/AR. As a first step, our model serves as a quantitative metric for evaluating and optimizing immersive applications, e.g., button layout in AR assistive tools or target positions in VR gaming.

In summary, our main contributions include:

- an EMG-sensed biometrical dataset of VR users' neck muscle activity, characterizing wide ranges of head movements,
- a biophysically formulated and learned model that predicts muscular contraction with head poses and movements,
- an extended metric that forecasts the viewing-induced muscular efforts and discomfort level given the target position,
- demonstrations of the model's effectiveness in enhancing users' muscle comfort via altering targets' spatial layouts.

2 RELATED WORK

2.1 Ergonomics in VR/AR Interaction

Ergonomic efficiency is essential to the mass adoption of VR/AR. Despite extensive efforts on designing more lightweight HMDs, their current form factors still considerably alter users' behaviors. Consequently, muscular discomfort [Chihara and Seo 2018; Forde et al. 2011; Penumudi et al. 2020; Souchet et al. 2022], especially in the neck and shoulders [Kim and Shin 2018; Marklin Jr et al. 2022], may be induced. Prior research has studied the impacts of head-supported mass on neck muscle activities under various application scenarios to better design dedicated hardware devices [Le et al. 2021; Rubine-Gatina et al. 2022; Thuresson et al. 2005, 2003], such as military helmets. Complementing advances in hardware designs, we focus on modeling and predicting muscle activities under the VR/AR settings, where visual stimuli are controllable and optimizable, to guide the design of virtual content for better ergonomic comfort. Our approach shares a similar mindset to [Li et al. 2020; Ruiz et al. 2018], i.e., task-dependent optimization of virtual content.

2.2 Muscle Contraction during Movements

Muscle contraction level is a core biometrical indicator for studying ergonomics [Dugan and Frontera 2000]. Unlike motions, which can be reliably tracked by cameras, quantifying muscle activities is notably more challenging. Existing work mainly exploits EMG to reveal muscle activities by detecting the electric signals propagating in neurally-activated muscles [Criswell 2010; Merletti and Parker 2004]. In particular, elevated EMG readings indicate stronger muscle contraction and elevated discomfort over time [Chesler and Durfee 1997; Cifrek et al. 2009; Dimitrova and Dimitrov 2003; Vigotsky et al. 2018]. Recently, researchers have explored machine learning techniques to infer muscle activities from spinal cord signals [Gok and Sahin 2019; Guo et al. 2018] and simulated human musculoskeletal animation data [Nakada et al. 2018].

2.3 Learning from Electromyography Signals

Learning EMG signals has emerged to understand human muscular behaviors with various applications [Ahsan et al. 2009; Atzori and Müller 2015; Phinyomark and Scheme 2018], including human-machine interfaces [Atzori et al. 2016; Karolus et al. 2022; Moon et al. 2005; Xiong et al. 2021] and VR/AR [Hirota et al. 2018; Lou et al. 2019; Pai et al. 2019; Tsuboi et al. 2017]. EMG data has also been leveraged to enable various sensing tasks, such as body movement [Baldacchino et al. 2018; Du et al. 2017; Jaramillo-Yánez et al. 2020; Javaid et al. 2021; Wei et al. 2019; Zhao et al. 2020], hand [Liu et al. 2021] and head [Barniv et al. 2005; Sugiarto et al. 2021] tracking. The flexible and non-invasive design of the latest EMG creates new possibilities for understanding our behaviors invisible to cameras. For instance, estimating force [Bardizbanian et al. 2020; Becker et al. 2018; Gailey et al. 2017; Martínez et al. 2020; Wu et al. 2021; Zhang et al. 2022], prosthetic [Castellini and Van Der Smagt 2009; Gulati et al. 2021] and gait [Nazmi et al. 2019; Papagiannis et al. 2019] control. We aim to achieve the inverse by predicting the EMG-measurable muscle status from human head movements.

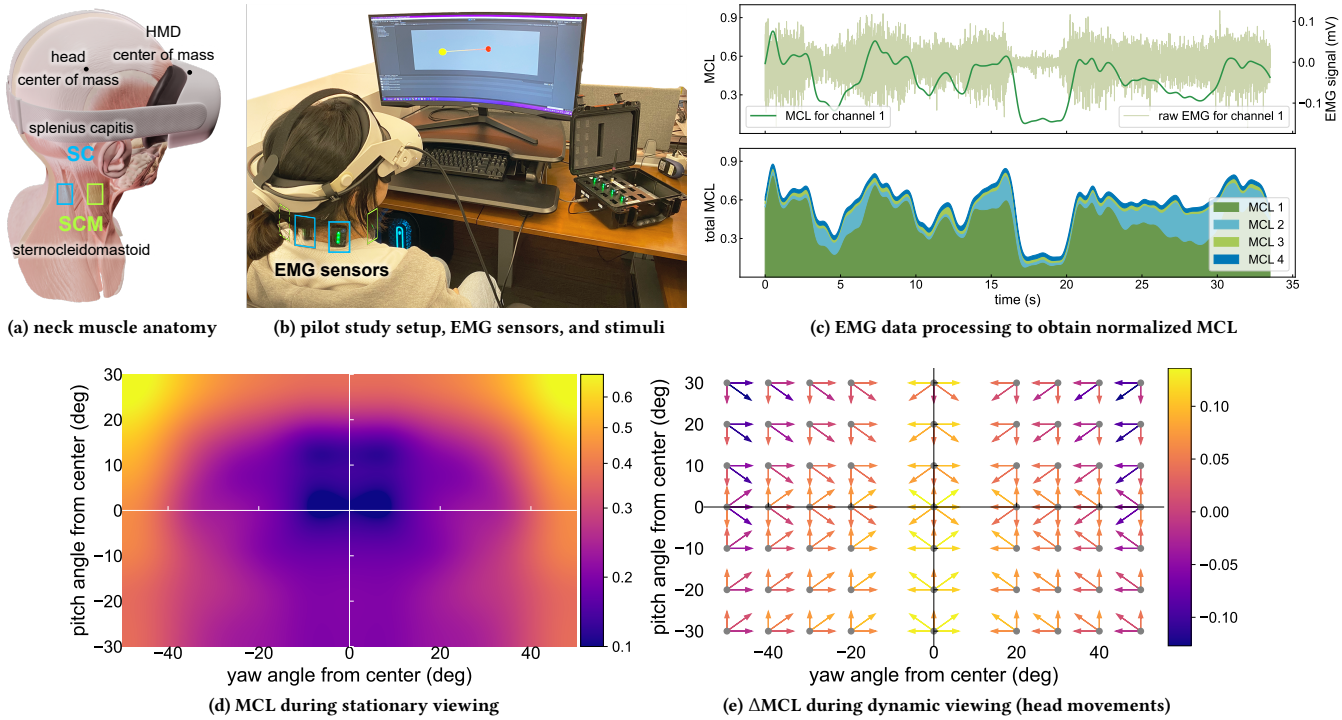

(a) neck muscle anatomy (b) pilot study setup, EMG sensors, and stimuli (c) EMG data processing to obtain normalized MCL

(d) MCL during stationary viewing (e) ΔMCL during dynamic viewing (head movements)

Figure 2: *Pilot study illustration and results.* (a) illustrates the major muscles controlling head movements, with highlighted EMG sensor attachment regions. (b) shows our experimental setup with EMG sensors annotated. (c) The top row shows an example raw EMG sequence (light green curve and right Y-axis) and its corresponding normalized MCL (dark green curve and left Y-axis). The bottom row shows the total MCL integrated across all 4 channels. (d) visualizes the user-aggregated MCL for stationary viewing. (e) shows the movement-induced ΔMCL for dynamic viewing. Each ΔMCL, i.e., arrow, was computed by subtracting the MCL during stationary viewing at an anchor head pose from the average MCL during head movement from that anchor head pose (arrow tail) to a target head pose (arrow head). The arrow lengths were scaled to 13% for easier visualization. 3D asset credits to joseVG and danielmclogan at Sketchfab.

3 NECK MUSCLE CONTRACTION LEVEL DURING HEAD MOVEMENTS IN VR

3.1 Neck Muscles Controlling Head Rotations

We aim to model and predict neck muscle contraction level (MCL). Human neck is a highly flexible skeletal structure that allows the head to change its pitch, yaw, and roll angles. As shown in Figure 2a, the major neck muscles include sternocleidomastoid (SCM) and splenius capitis (SC) [Vasavada et al. 1998]. In particular, SCM/SC laterally rotate the head to the opposite/same side when acting unilaterally and flex/extend the head when acting bilaterally.

3.2 Experiment Description

Participants and setup. We recruited 8 participants (ages 23 – 31, 3 female). 4 of them have prior experience with VR headsets before the study. All participants reported normal neck muscle conditions. For each participant, we attached 4 Delsys Trigno wireless EMG sensors on the left/right SCM and SC muscles (see Figures 2a and 2b). We originally tested with 6 EMG sensors by also including the upper trapezius (UT) muscles. However, EMG sensors on the UT exhibited significantly weaker signals compared to the others and were thus excluded from the experiments. The EMG sensors detect the electric potential (in millivolts, mV) generated by users' muscle fibers at 2000 Hz and stream the data to a PC with $<$ 1ms latency. During the study, every participant wore an Oculus Quest 2 head-mounted display (HMD), remained seated, and performed a target reaching task with visual stimuli. Their head poses were tracked by the HMD and streamed to the same PC for time synchronization with EMG. The HMD provides 1872×1856 resolution per eye at 90 FPS, and $98°/104°$ vertical/horizontal field of view (FoV).

Stimuli and tasks. As illustrated in Figure 2b, the stimuli were sequentially displayed pairs of spheres (3° in the FoV), one colored yellow and the other red. The yellow sphere indicates an "anchor" head pose $\mathbf{r} \triangleq (p, y)$, where p/y represent pitch and yaw angles. The red sphere indicates a "target" head pose that is $\mathbf{\Delta r} \triangleq (\Delta p, \Delta y)$ away from $\mathbf{r}$. While keeping their torso stationary, participants were instructed to rotate their heads from the yellow anchor to the red target. Once the user successfully fixated on the target for 2 seconds consecutively (simulating stationary viewing), both spheres were shifted to continue with the next trial. A line connecting the two spheres was rendered to guide the user's head rotation to the next target, designed to eliminate potential errors for target searching. Please refer to our video for an example of the study process.

Conditions. Across participants, the stimuli pairs appeared randomly with a pre-sampled anchor set $\mathcal{R} \triangleq \{(\mathbf{r}_i, \Delta\mathbf{r}_i), i = 1, \dots N_{\mathcal{R}}\}$. Given the comfortable range of human head rotations [Ruiz et al. 2018], we sampled stimulus directions within a $60^\circ \times 100^\circ$ visual field. We tested and chose not to cover additional vertical range to ensure participants' neck comfort and avoid sprains. We started with a preliminary test to determine the effective range of $\mathbf{r}$. Our test with 3 participants showed non-trivial EMG change for $|y| > 15^\circ$ and $|p| > 5^\circ$. Therefore, using a 10° step size, we sampled 63 anchor head poses for $p \in \{\pm 30^\circ, \pm 20^\circ, \pm 10^\circ, 0^\circ\}$ and $y \in \{\pm 50^\circ, \pm 40^\circ, \pm 30^\circ, \pm 20^\circ, 0^\circ\}$. Here, $-/+$ indicates left/right or down/up from the head's forward-facing direction. For each of the 63 anchor poses $\mathbf{r}$, 8 surrounding targets giving varying movement patterns $\Delta\mathbf{r}$ were studied. They were selected with $\Delta p \in \{\pm 35^\circ, 0\}, \Delta y \in \{\pm 25^\circ, 0\}$. We discarded the conditions with target stimuli outside of the $60^\circ \times 100^\circ$ range. That is, we ensured $\mathbf{r} + \Delta\mathbf{r} \in [-30^\circ, +30^\circ] \times [-50^\circ, +50^\circ]$.

Duration. We split the study into 7 sessions (about 5 minutes each) with enforced breaks in between to avoid posture drifting. Every session was monitored to ensure the subject remained stationary below the neck. The study, including hardware setup, pre-study instructions, warm-up session (30 discarded trials), and breaks, took about 2.5 hours per participant. In total, we collected about 5 hours of time-synchronized motion-EMG paired data.

Data processing and analysis. We aim to model and optimize neck muscle contraction driving head movements. However, raw EMG signals cannot be directly used because they exhibit: 1) frequency-dependent sensory noise; 2) oscillations between negative and positive values; 3) left-right asymmetry due to sensor positioning error [Chihara and Seo 2018; Lehman and McGill 1999]; 4) cross-user difference in scale for the same head movement. Therefore, similar to prior literature [Reaz et al. 2006; Sommerich et al. 2000], we performed a series of EMG signal processing, including detrending, bandpass filtering, and rectification, as well as inter-channel balancing, normalization, and integration. Please refer to Supplement A for details. At each time frame, our processing pipeline outputs a single normalized muscle contraction value, integrated across processed EMG signals from all 4 channels. Figure 2c illustrates the EMG-to-MCL transformation with an example sequence.

3.3 Results

Stationary viewing ($|\Delta\mathbf{r}| = 0$). Figure 2d shows the MCL when the head remains static. The average normalized MCL was $.32 \pm .12$. The head pose demanding the least MCL ($.17 \pm .02$) was $\mathbf{r} = (0, 0)$, significantly lower than far-reaching poses. For instance, when the target was located at $\mathbf{r} = (30^\circ, 50^\circ)$, the MCL was higher at $.68 \pm .09$. A repeated measures ANOVA showed that both p and y had a significant main effect on MCL ($F_{6,42} = 1.17, p < .001$ for p, $F_{8,56} = 1.5, p < .001$ for y). A significant $p \times y$ interaction effect was also observed ($F_{48,336} = 7.4, p < .001$). In particular, higher absolute values of yaw elevate the corresponding average MCL, from $.21 \pm .09$ with $y = 0^\circ$ to $.47 \pm .15$ with $|y| = 50^\circ$. A Mann-Kendall (M.K.) trend test showed a significant monotonic trend ($\tau = 1.0, p < .05$). On the other hand, the effect from pitch was asymmetric and non-monotonic. The highest values of p, $p = +30^\circ / -30\circ$ induces MCL at $.49 \pm .16 / .27 \pm .09$. An M.K. trend test did not show a significant monotonic trend of pitch angle's effect on MCL ($\tau = -.6, p = .07$).

Dynamic viewing ($|\Delta\mathbf{r}| > 0$). Figure 2e visualizes the ΔMCL during head movements, which was computed by subtracting the stationary MCL at an anchor from the average MCL during the movement. Introducing movements (i.e., non-zero $\Delta\mathbf{r}$) significantly elevated MCL up to 31.21% across all studied $\mathbf{r}$. In addition to $\mathbf{r}$, movement pattern $\Delta\mathbf{r}$ jointly influences the observed MCL. A repeated measures ANOVA showed that $\Delta p \times \Delta y$ has a significant main effect on MCL ($F_{3,21} = 23.44, p < .001$). For each time frame, we further extracted the angular acceleration in both directions $\boldsymbol{\alpha} \triangleq (\boldsymbol{\alpha}_p, \boldsymbol{\alpha}_y)$. Pearson correlation coefficients were computed to assess the relationship; There were positive correlations between MCL and $|\boldsymbol{\alpha}_p|$ ($r(12431) = .14, p < .001$), as well as MCL and $|\boldsymbol{\alpha}_y|$ ($r(12431) = .038, p < .001$). The elevation rate depends on individual $\mathbf{r}$. For example, the rate in yaw direction with movement starting at $\mathbf{r} = (30^\circ, 50^\circ)$ was 88.9% higher than $\mathbf{r} = (0^\circ, 0^\circ)$.

3.4 Discussion

The analysis above leads us to several observations and motivations for learning a computational model. First, despite individual participants' variances in muscular strengths and sizes, the measured MCL shares consistent trends for each condition, both during static viewing and dynamic movements. Second, the head pose (yaw y and pitch p) significantly influences MCL. In particular, despite the left-right symmetry with yaw, the pitch angle exhibits significantly asymmetric and non-monotonic effects on MCL. Lower pitch angles (i.e., heads facing downward) tend to reduce MCL. Third, in dynamic scenarios, increasing acceleration significantly elevates MCL. The elevation effect size depends on both the corresponding starting head pose and movement direction.

4 METHOD: MODELING AND PREDICTING NECK MUSCLE CONTRACTION LEVEL

The analysis of EMG-motion paired data from our pilot study motivates us to establish a computational model correlating head movements with neck muscle contraction level (MCL). Note that while MCL can be measured using EMG sensors, they are 1) tedious and costly to deploy; 2) insufficient to *forecast* MCL before a movement happens. Therefore, we first propose a bio-physically inspired MCL estimation model with open functions to characterize muscle-driven head motions in Section 4.1. Using our collected data, we then fit the open functions with machine learning models to:

(1) estimate the MCL associated with a completed head movement, i.e., *after* a movement happens (Section 4.2);
(2) predict the MCL for a potential movement using target directions only, i.e., *before* a movement happens (Section 4.3).

4.1 Bio-Physically Inspired MCL Model

Muscle-generated torque is proportional to MCL [Clancy et al. 2011; Paquin and Power 2018; Watanabe and Akima 2009]. Our neck muscles actively generate the required amount of torque to enable head rotation at varying speeds. Denoting this **a**ctive torque as $\mathcal{T}_\mathbf{a} \in \mathbb{R}^2$, we establish a mapping $\mathcal{E}(\cdot)$ such that MCL $= \mathcal{E}(\mathcal{T}_\mathbf{a})$.

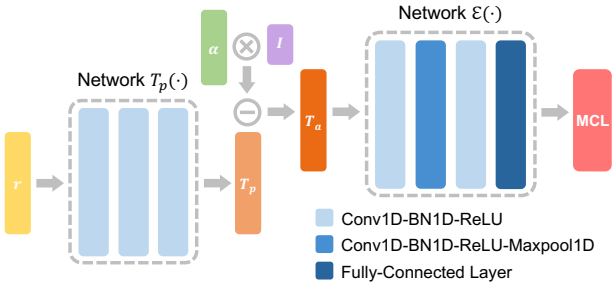

(a) illustration of MCLNet's architectural design

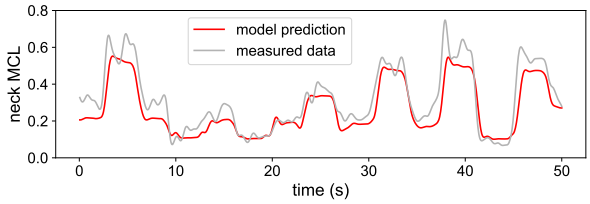

(b) model-predicted vs. hardware-measured neck MCL

Figure 3: *MCLNet illustration and example MCL estimation results.* (a) illustrates the architectural design of MCLNet for jointly learning I, $\mathcal{T}_\mathbf{p}(\cdot)$, and $\mathcal{E}(\cdot)$ from head motion and MCL paired data; (b) shows the model-predicted vs. hardware-measured MCL for a sample sequence from the test set.

From our pilot study (Figure 2d), maintaining the head stationary at various poses requires significantly different levels of MCL, and thus $\mathcal{T}_\mathbf{a}$. To maintain stationary viewing, however, there must be another pose-dependent torque that counterbalances $\mathcal{T}_\mathbf{a}$. We term this underlying torque as **p**assive torque $\mathcal{T}_\mathbf{p} \in \mathbb{R}^2$. We hypothesize that $\mathcal{T}_\mathbf{p}$ is induced by factors such as gravity and muscle relaxation. Notably, $\mathcal{T}_\mathbf{p}$ exists during both stationary and dynamic viewing conditions, but only depends on head poses, i.e., $\mathcal{T}_\mathbf{p} \triangleq \mathcal{T}_\mathbf{p}(\mathbf{r})$. By contrast, we proactively generate $\mathcal{T}_\mathbf{a}$ to perform stationary viewing (compensating $\mathcal{T}_\mathbf{p}$) and change our head pose at wish for dynamic viewing. Therefore, through the moment of inertia $I \in \mathbb{R}$, $\mathcal{T}_\mathbf{a}$ correlates both with the head pose $\mathbf{r}$ and angular acceleration $\boldsymbol{\alpha}$:

$$\mathcal{T}_\mathbf{p}(\mathbf{r}) + \mathcal{T}_\mathbf{a}(\mathbf{r}, \boldsymbol{\alpha}) = I \times \boldsymbol{\alpha}. \tag{1}$$

This further transforms the mapping $\mathcal{E}(\cdot)$ between $\mathcal{T}_\mathbf{a}$ and MCL:

$$\begin{aligned} \text{MCL} &= (\mathcal{E} \circ \mathcal{T}_\mathbf{a})(\mathbf{r}, \boldsymbol{\alpha}) = \mathcal{E}\left(I \times \boldsymbol{\alpha} - \mathcal{T}_\mathbf{p}(\mathbf{r})\right) \\ &\triangleq \mathcal{H}_m\left(\mathcal{E}, \mathcal{T}_\mathbf{p}, I, \mathbf{r}, \boldsymbol{\alpha}\right) \mapsto \mathbb{R}^+, \end{aligned} \tag{2}$$

where I, $\mathcal{T}_\mathbf{p}(\cdot)$, and $\mathcal{E}(\cdot)$ are the unknowns that map $\mathbf{r}/\boldsymbol{\alpha}$ to MCL.

4.2 Estimating MCL with Complete Trajectories

The data from our pilot study provide a large set of time-synchronized head movement trajectories and MCL sequences:

$$\mathbf{r}_t, \boldsymbol{\alpha}_t \mapsto \mathcal{H}_m\left(\mathcal{E}, \mathcal{T}_\mathbf{p}, I, \mathbf{r}_t, \boldsymbol{\alpha}_t\right). \tag{3}$$

Using these paired sequential data, we formulate an MCL regression problem and optimize 1D CNN models with L_2 loss to jointly approximate the unknowns I, $\mathcal{T}_\mathbf{p}(\cdot)$, and $\mathcal{E}(\cdot)$. The complete model, named *MCLNet*, is illustrated in Figure 3a.

Notably, a phenomenon called electro-mechanical delay exists between EMG signals and muscular motions. Depending on individuals and muscle areas, the delay can incur a temporal offset between the two modalities up to 100ms [Cavanagh and Komi 1979]. To accommodate this temporal inconsistency for robust prediction, our model takes in motion sequences with T=400ms window and predicts MCL for the central 200ms interval, i.e., inputs cover additional 100ms outputs from the beginning and end. Given a sequence of uniformly sampled head poses $\{\mathbf{r}^t\}_{t=1}^T$, we first calculate the corresponding angular accelerations $\{\boldsymbol{\alpha}^t\}_{t=1}^T$ through finite difference, then execute our model at each t to obtain the overlapping sequences of predicted MCL. Figure 3b visualizes the prediction-measurement comparison for an example trajectory taken from the test set. Visualized results for each subject are shown in Figure 8.

So far, a core requirement of MCLNet is the prior knowledge of completed head movement trajectories. However, to benefit real-life applications such as UX design and cinematography, we shall reduce the potential discomfort before deploying to users. To this end, we further extend our model to *forecast* MCL before a movement.

4.3 Predicting MCL with Target Head Poses

Given the starting and ending head poses $\{\mathbf{r_s}, \mathbf{r_e}\}$ of a uni-directional head movement, the required MCL to travel between them is determined by the actual movement trajectory. However, as evidenced by our analysis in Section 3.4, $\{\mathbf{r_s}, \mathbf{r_e}\}$ alone carry significant influence on the overall MCL. Therefore, using our collected data, we regress a representative motion trajectory for each pair of $\{\mathbf{r_s}, \mathbf{r_e}\}$, to approximate the temporal patterns of angular velocity $\boldsymbol{\omega}_t$:

$$\boldsymbol{\omega}_t(\mathbf{r_s}, \mathbf{r_e}) \in \mathbb{R}^2, \ \text{ s.t. } \mathbf{r_s} + \int_{t=t_s}^{t_e} \boldsymbol{\omega}_t(\mathbf{r_s}, \mathbf{r_e}) \mathrm{d}t = \mathbf{r_e}. \tag{4}$$

Motivated by prior literature studying the main sequence effect of head movements [Zangemeister et al. 1981] and our observations of a single main peak in each velocity profile (Figure 4), we perform a unimodal Gaussian approximation for the angular velocity:

$$\boldsymbol{\omega}_t^i(\mathbf{r_s}, \mathbf{r_e}) \triangleq A^i(\mathbf{r_s}, \mathbf{r_e}) e^{-\frac{\left(t-\mu^i(\mathbf{r_s},\mathbf{r_e})\right)^2}{2\left(\sigma^i(\mathbf{r_s},\mathbf{r_e})\right)^2}}, i \in \{p, y\}. \tag{5}$$

Using our collected data, we formulate a trajectory regression problem and optimize a Multi-Layer Perceptron (MLP) model, annotated as *TrajectoryNet*, to predict $\{A^i, \mu^i, \sigma^i\}_{i\in\{p,y\}}$ given an arbitrary pair of head poses $\{\mathbf{r_s}, \mathbf{r_e}\}$. Using predicted angular velocity curves, we can approximate the overall MCL:

$$\mathrm{H}_c(\mathbf{r_s}, \mathbf{r_e}) = \int_{t=t_s}^{t_e} \mathcal{H}_m\left(\mathcal{E}, \mathcal{T}_\mathbf{p}, I, \mathbf{r_s} + \int_{\bar{t}=t_s}^{t} \boldsymbol{\omega}_{\bar{t}}(\mathbf{r_s}, \mathbf{r_e}) \mathrm{d}\bar{t}, \dot{\boldsymbol{\omega}}_t\right) \mathrm{d}t. \tag{6}$$

Figure 4 compares the velocity curves collected from our users with TrajectoryNet's predictions over an example pair of $\{\mathbf{r_s}, \mathbf{r_e}\}$ taken from the test set. Full implementation details for both MCLNet and TrajectoryNet can be found in Supplement B.

5 EVALUATION

We present a series of objective measurements on our model's performance in predicting neck MCL, and a subjective psychophysical study to demonstrate how the prediction reflects neck muscle discomfort. We first evaluate MCLNet's estimation accuracy with

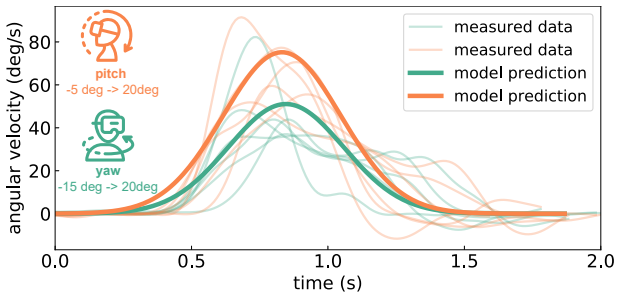

Figure 4: *Predicting head motion trajectories with starting/ending head poses.* Light/dark curves show tracked/predicted angular velocities. Orange/green curves show angular velocities in pitch/yaw directions.

complete head motion trajectories in Section 5.1, then extend to predict MCL *before* head movements by incorporating TrajectoryNet in Section 5.2. Through a user study, we demonstrate our method's potential in forecasting and reducing users' neck workload for a more comfortable VR experience in Section 5.3.

5.1 MCL Estimation: After Head Movements

Experimental setup. We leveraged our data from the conditions detailed in Section 3.2 to train our model. Additionally, during the pilot study, we also collected two groups of conditions to establish an evaluation dataset with unseen conditions. It contains 4 pitch and 4 yaw angles, $p \in \{\pm 25^\circ, \pm 5^\circ\}, y \in \{\pm 45^\circ, \pm 15^\circ\}$, resulting in a total of 16 anchor head poses. The same 8 surrounding targets with travel angle $\Delta p \in \{\pm 35^\circ, 0^\circ\}, \Delta y \in \{\pm 25^\circ, 0^\circ\}$ were introduced to each of them. Note that the evaluation conditions were designed to contain no overlap with the training set. Due to the extra long collection process and thus scheduling conflicts, 6 (3 female) of the 8 participants completed the evaluation condition session. We adopted their data for this experiment. Two quantitative metrics were considered: Normalized Root-Mean-Square Error (NRMSE) and Normalized Mean Absolute Error (NMAE). The metrics are applied to measure the error ratio between the model-predicted and hardware-measured (by the same method detailed in Supplement A) MCL; a lower error ratio indicates better model performance.

Results and discussion. MCLNet achieves an overall performance of 12.39 ± 4.74% NRMSE and 9.54 ± 4.14% NMAE across all 6 subjects and 16 anchor head poses. Figure 6 summarizes its subject-wise performance. Beyond the average accuracy, we further measure the correlation. That is, whether the model can predict the elevation/reduction of MCL consistently with the hardware measurement. We leveraged Pearson's and Spearman's coefficients between the two conditions. The results indicate a significant correlation between model predictions and hardware measurements ($r(70066) = .62, p < .001$ and $r(70066) = .60, p < .001$). The analyzes above validate our method's effectiveness in estimating neck MCL when head motion trajectories were known beforehand.

5.2 MCL Prediction: Before Head Movements

Experimental setup. For this experiment, we first used the head motion data from Section 5.1 to optimize and validate TrajectoryNet (Section 4.3), then combined it with MCLNet to predict MCL using target head poses only. Since our dataset consists of sequences of stationary head pose followed by pose-changing movements, we extracted the dynamic part to construct a dataset of starting/ending head poses $\{\mathbf{r_s}, \mathbf{r_e}\}$ paired with HMD-tracked trajectories. The train-test data split from Section 5.1 was used for evaluation.

Results and discussion. The performance of our MCL prediction framework, composed of trajectory regression and MCL estimation, is shown in Figure 7. TrajectoryNet achieves an overall NRMSE/NMAE of 3.54 ± 1.11%/2.16 ± 0.65% in pitch velocity and 3.45 ± 0.98%/2.01 ± 0.51% in yaw. The overall MCL prediction performance is 16.76 ± 6.05% NRMSE and 14.71 ± 5.96% NMAE. Pearson's and Spearman's coefficients between the two conditions are $r(70066) = .59, p < .001$ and $r(70066) = .57, p < .001$, indicating a significant correlation. The results above demonstrate that our method can reliably predict the potential MCL with only the target head poses, before the actual movement occurs.

5.3 Predicting and Reducing Neck Discomfort

Participants and setup. We recruited 13 participants (ages 20 – 35, 6 female). None of them were aware of the hypothesis, the research, or the number of conditions. One participant came in with a prior condition of neck injury and was excluded during warm-up sessions. There was no overlap between these participants and those from the pilot study in Section 3. We conducted the study using an Oculus Quest 2 HMD (*without EMG*). During the study, participants observed stimuli through the HMD and were instructed to remain seated while keeping their torso stationary. The study took around 60 minutes for each participant, including breaks between sessions.

Stimuli. As shown in Figure 5a, we developed and experimented with a 3D balloon-popping game with target acquisition. The stimuli were displayed as a sequence of red balloon targets rendered in an amusement park scene. As an indicator, the target color was changed to magenta upon a participant's fixation. A line pointing toward the next target was displayed to guide the user.

Tasks. The task was designed as two-alternative forced choice to avoid bias from scaled rating, similar to prior works measuring muscular discomfort [Farid et al. 2018; Pinto et al. 2021]. During each session, the balloon targets were displayed, one at a time, following a pre-defined scan path with 31 targets in different directions $\mathcal{S} = \{\mathbf{r}_t, t = 0, \ldots, 30, \mathbf{r}_i \in \mathcal{R}\}$, similar to the definition in Section 3.2. Participants were instructed to rotate their heads to fixate on the balloon until it disappeared. To trigger both dynamic and stationary head status, a 1-second fixation on each target was enforced before the next one appeared at $\mathbf{r}_{t+1}$. Each session contained a pair of two sequentially tested $\mathcal{S}$ that were generated from 2 out of 3 different conditions, as detailed in the *conditions* paragraph. After each session, the participants were instructed to use the keyboard to indicate "which one of the two scan paths was more uncomfortable, tiring, or difficult for your neck?".

Conditions. Guided by our model, we designed 3 conditions of progressively generated scan paths. They were created to ensure an identical total head rotations and similar spatial coverage but

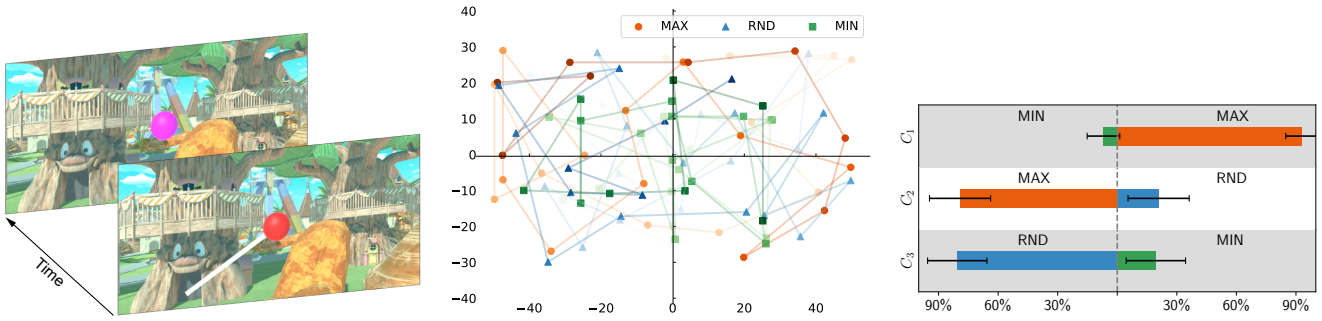

(a) setting and stimuli (b) visualization of conditions (c) aggregated voting results

Figure 5: *Stimuli and results of our neck discomfort user study.* (a) shows the stimuli. (b) visualizes the visual targets' angular distributions of 3 example conditions. Color gradients indicate the temporal order of appearance. All 3 conditions share the same total head rotations with full visual field coverage. (c) summarizes the voting distribution of the 3 comparisons on which condition being more uncomfortable. Individual votes per condition are detailed in Table 1. 3D asset credits to Mixall at Unity.

varied cumulative MCL. To ensure fair movements across conditions, we randomly pre-partitioned a fixed amount of total head rotations 900° into 30 steps. Then, at each step t, the next target pose $\mathbf{r}_{t+1}$ was chosen from a set of candidate poses by maximizing the corresponding score function of the selected condition:

$$\begin{aligned} \textbf{MAX}&: \mathrm{C}(\mathbf{r}_{i\in[1,t+1]}) + \mathrm{H}_c(\mathbf{r}_t, \mathbf{r}_{t+1}) \\ \textbf{RND}&: \mathrm{C}(\mathbf{r}_{i\in[1,t+1]}) \\ \textbf{MIN}&: \mathrm{C}(\mathbf{r}_{i\in[1,t+1]}) - \mathrm{H}_c(\mathbf{r}_t, \mathbf{r}_{t+1}) \end{aligned}$$

Here, C is a term to ensure full visual field coverage for condition-wise fairness. On average, the ratio between the cumulative MCL of the three conditions **MAX**/**RND**/**MIN** was 3.48 vs. 1.95 vs. 1.00. Please refer to Supplement D for details on our condition generation algorithm and Figure 5b for an example of each condition. The three conditions generate 3 different pairs for 2AFC comparisons, namely $\mathbf{C_1}$: **MAX** vs. **MIN**; $\mathbf{C_2}$: **RND** vs. **MAX**; $\mathbf{C_3}$: **MIN** vs. **RND**. We repeated the random pre-partition of total head rotations and condition generation process to get 6 sets of **MAX**/**RND**/**MIN** conditions for a total of 18 sessions. The appearance order of the 18 sessions was randomized and counter-balanced across participants, same for the 2 conditions within each session, to avoid bias.

Results. Table 1 in Supplement E and Figure 5c show individual votes and the summary for each comparison, respectively. By aggregating all sessions, **MAX**/**RND**/**MIN** were 86.1%/50.7%/13.1% voted as being more uncomfortable in the related comparisons. Among all comparisons, The difference was significantly higher than a random guess (50%). By analyzing individual votes, a repeated measures ANOVA indicated that the condition had a statistically significant effect on the votes ($F_{2,22} = 89.46, p < .001$). Post-hoc pairwise t-tests with Holm adjustments showed that the difference was significant among all 3 comparisons ($p < .001$ for all conditions).

Discussion. The analysis above shows the significant difference in participants' subjectively perceived discomfort levels among the three conditions. The participant-rated discomfort levels, **MAX** > **RND** > **MIN**, also matched our model's prediction (H_c). Note that the significant difference was not induced by head rotation angles which were ensured to be identical via our progressive trajectory generation. These results demonstrated our model's capability of predicting a user's neck discomfort with target head poses only, i.e., before the head movement takes place.

6 LIMITATIONS AND FUTURE WORK

This work considered the influence of yaw and pitch angles on MCL, but not the roll dimension due to the challenges of precisely manipulating it with visual stimuli and natural head movements. However, it may also contribute to MCL [Keshner et al. 1989]. Introducing alternative tasks, such as full body movement [Imai et al. 2001], may enable controlling roll angles. We plan to investigate the options concerning their effects on noise and movement naturalness. Similar extensions include other muscle groups, such as shoulders during interaction [Chihara and Seo 2018].

In Section 4.3, we estimate the motion trajectory speed as a Gaussian representation given a starting and ending head pose. Despite the representativeness [Hage et al. 2019], the approximation may not fully contain the individuals' behavioral variances. We envision probabilistic modeling and learning [Ghahramani 2015] may further reveal the statistical variances across users.

7 CONCLUSION

Using EMG sensors, we present biometrically-measured data that reveals VR users' neck muscular contraction levels and thus potential discomfort. By leveraging the data, we learn a computational model that quantitatively predicts the MCL, both after and before a head movement occurs. We hope the research to motivate new ergonomic and health-aware designs for VR/AR and interactive computer graphics, toward answering essential questions such as "will VR/AR devices induce additional ergonomic burdens on users if they replace smartphones and monitors for everyday usage?", "how do we theoretically design more comfortable immersive displays and interfaces before they are deployed?". To this end, our model may be applied to ergonomic-aware VR/AR interface optimization, immersive video editing, and beyond.

ACKNOWLEDGMENTS

This project is partially supported by the National Science Foundation grants #2225861 and #2232817, and a DARPA PTG program.

REFERENCES

Md Rezwanul Ahsan, Muhammad I Ibrahimy, Othman O Khalifa, et al. 2009. EMG signal classification for human computer interaction: a review. *European Journal of Scientific Research* 33, 3 (2009), 480–501.

Manfredo Atzori, Matteo Cognolato, and Henning Müller. 2016. Deep learning with convolutional neural networks applied to electromyography data: A resource for the classification of movements for prosthetic hands. *Frontiers in neurorobotics* 10 (2016), 9.

Manfredo Atzori and Henning Müller. 2015. The Ninapro database: a resource for sEMG naturally controlled robotic hand prosthetics. In *2015 37th Annual International Conference of the IEEE Engineering in Medicine and Biology Society (EMBC)*. IEEE, 7151–7154.

A T Bahill, D Adler, and L Stark. 1975. Most naturally occurring human saccades have magnitudes of 15 degrees or less. *Investigative Ophthalmology & Visual Science* 14, 6 (06 1975), 468–469. arXiv:https://arvojournals.org/arvo/content_public/journal/iovs/933061/468.pdf

Tara Baldacchino, William R Jacobs, Sean R Anderson, Keith Worden, and Jennifer Rowson. 2018. Simultaneous force regression and movement classification of fingers via surface EMG within a unified Bayesian framework. *Frontiers in bioengineering and biotechnology* 6 (2018), 13.

Berj Bardizbanian, Jennifer Keating, Xinming Huang, and Edward A Clancy. 2020. Estimating Individual and Combined Fingertip Forces From Forearm EMG During Constant-Pose, Force-Varying Tasks. In *2020 42nd Annual International Conference of the IEEE Engineering in Medicine & Biology Society (EMBC)*. IEEE, 3134–3137.

Yair Barniv, Mario Aguilar, and Erion Hasanbelliu. 2005. Using EMG to anticipate head motion for virtual-environment applications. *IEEE Transactions on Biomedical Engineering* 52, 6 (2005), 1078–1093.

Vincent Becker, Pietro Oldrati, Liliana Barrios, and Gábor Sörös. 2018. Touchsense: classifying finger touches and measuring their force with an electromyography armband. In *Proceedings of the 2018 ACM International Symposium on Wearable Computers*. 1–8.

Geoffrey L Brown, Nidhi Seethapathi, and Manoj Srinivasan. 2021. A unified energy-optimality criterion predicts human navigation paths and speeds. *Proceedings of the National Academy of Sciences* 118, 29 (2021), e2020327118.

Claudio Castellini and Patrick Van Der Smagt. 2009. Surface EMG in advanced hand prosthetics. *Biological cybernetics* 100, 1 (2009), 35–47.

Peter R Cavanagh and Paavo V Komi. 1979. Electromechanical delay in human skeletal muscle under concentric and eccentric contractions. *European journal of applied physiology and occupational physiology* 42, 3 (1979), 159–163.

Yumiao Chen, Xin Wang, and Huijia Xu. 2021. Human factors/ergonomics evaluation for virtual reality headsets: a review. *CCF Transactions on Pervasive Computing and Interaction* 3, 2 (2021), 99–111.

Naomi C Chesler and William K Durfee. 1997. Surface EMG as a fatigue indicator during FES-induced isometric muscle contractions. *Journal of Electromyography and Kinesiology* 7, 1 (1997), 27–37.

Takanori Chihara and Akihiko Seo. 2018. Evaluation of physical workload affected by mass and center of mass of head-mounted display. *Applied ergonomics* 68 (2018), 204–212.

Mario Cifrek, Vladimir Medved, Stanko Tonković, and Saša Ostojić. 2009. Surface EMG based muscle fatigue evaluation in biomechanics. *Clinical biomechanics* 24, 4 (2009), 327–340.

Edward A Clancy, Lukai Liu, Pu Liu, and Daniel V Zandt Moyer. 2011. Identification of constant-posture EMG–torque relationship about the elbow using nonlinear dynamic models. *IEEE Transactions on Biomedical Engineering* 59, 1 (2011), 205–212.

Eleanor Criswell. 2010. *Cram's introduction to surface electromyography*. Jones & Bartlett Publishers.

NA Dimitrova and GV Dimitrov. 2003. Interpretation of EMG changes with fatigue: facts, pitfalls, and fallacies. *Journal of Electromyography and Kinesiology* 13, 1 (2003), 13–36.

Yu Du, Yongkang Wong, Wenguang Jin, Wentao Wei, Yu Hu, Mohan S Kankanhalli, and Weidong Geng. 2017. Semi-Supervised Learning for Surface EMG-based Gesture Recognition.. In *IJCAI*. 1624–1630.

Sheila A Dugan and Walter R Frontera. 2000. Muscle fatigue and muscle injury. *Physical medicine and rehabilitation clinics of North America* 11, 2 (2000), 385–403.

Bassem Farid, Paul Yielder, Michael Holmes, Heidi Haavik, and Bernadette A Murphy. 2018. Association of subclinical neck pain with altered multisensory integration at baseline and 4-week follow-up relative to asymptomatic controls. *Journal of manipulative and physiological therapeutics* 41, 2 (2018), 81–91.

Farshad Farshadmanesh, Patrick Byrne, Hongying Wang, Brian D Corneil, and J Douglas Crawford. 2012. Relationships between neck muscle electromyography and three-dimensional head kinematics during centrally induced torsional head perturbations. *Journal of Neurophysiology* 108, 11 (2012), 2867–2883.

Kelsey A Forde, Wayne J Albert, Michael F Harrison, J Patrick Neary, James Croll, and Jack P Callaghan. 2011. Neck loads and posture exposure of helicopter pilots during simulated day and night flights. *International Journal of Industrial Ergonomics* 41, 2 (2011), 128–135.

Alycia Gailey, Panagiotis Artemiadis, and Marco Santello. 2017. Proof of concept of an online EMG-based decoding of hand postures and individual digit forces for prosthetic hand control. *Frontiers in neurology* 8 (2017), 7.

Zoubin Ghahramani. 2015. Probabilistic machine learning and artificial intelligence. *Nature* 521, 7553 (2015), 452–459.

Sinan Gok and Mesut Sahin. 2019. Prediction of forelimb EMGs and movement phases from corticospinal signals in the rat during the reach-to-pull task. *International journal of neural systems* 29, 07 (2019), 1950009.

Paras Gulati, Qin Hu, and S Farokh Atashzar. 2021. Toward Deep Generalization of Peripheral EMG-Based Human-Robot Interfacing: A Hybrid Explainable Solution for NeuroRobotic Systems. *IEEE Robotics and Automation Letters* 6, 2 (2021), 2650–2657.

Yi Guo, Sinan Gok, and Mesut Sahin. 2018. Convolutional networks outperform linear decoders in predicting EMG from spinal cord signals. *Frontiers in neuroscience* 12 (2018), 689.

Renaud Hage, Fabien Buisseret, Laurent Pitance, Jean-Michel Brismée, Christine Detrembleur, and Frédéric Dierick. 2019. Head-neck rotational movements using DidRen laser test indicate children and seniors' lower performance. *PloS one* 14, 7 (2019), e0219515.

Mamoru Hirota, Ayumu Tsuboi, Masayuki Yokoyama, and Masao Yanagisawa. 2018. Gesture recognition of air-tapping and its application to character input in VR space. In *SIGGRAPH Asia 2018 Posters*. 1–2.

Kalman E Holdy. 2004. Monitoring energy metabolism with indirect calorimetry: instruments, interpretation, and clinical application. *Nutrition in Clinical Practice* 19, 5 (2004), 447–454.

Takao Imai, Steven T Moore, Theodore Raphan, and Bernard Cohen. 2001. Interaction of the body, head, and eyes during walking and turning. *Experimental brain research* 136, 1 (2001), 1–18.

Andrés Jaramillo-Yánez, Marco E Benalcázar, and Elisa Mena-Maldonado. 2020. Real-time hand gesture recognition using surface electromyography and machine learning: a systematic literature review. *Sensors* 20, 9 (2020), 2467.

Haider Ali Javaid, Mohsin Islam Tiwana, Ahmed Alsanad, Javaid Iqbal, Muhammad Tanveer Riaz, Saeed Ahmad, and Faisal Abdulaziz Almisned. 2021. Classification of Hand Movements Using MYO Armband on an Embedded Platform. *Electronics* 10, 11 (2021), 1322.

Jakob Karolus, Simon Thanheiser, David Peterson, Nicolas Viot, Thomas Kosch, Albrecht Schmidt, and Paweł W Wozniak. 2022. Imprecise but Fun: Playful Interaction Using Electromyography. *Proceedings of the ACM on Human-Computer Interaction* 6, MHCI (2022), 1–21.

Emily A Keshner, D Campbell, RT Katz, and BW Peterson. 1989. Neck muscle activation patterns in humans during isometric head stabilization. *Experimental Brain Research* 75, 2 (1989), 335–344.

Eunjee Kim and Gwanseob Shin. 2018. Head rotation and muscle activity when conducting document editing tasks with a head-mounted display. In *Proceedings of the Human Factors and Ergonomics Society Annual Meeting*, Vol. 62. SAGE Publications Sage CA: Los Angeles, CA, 952–955.

James F Knight and Chris Baber. 2004. Neck muscle activity and perceived pain and discomfort due to variations of head load and posture. *Aviation, space, and environmental medicine* 75, 2 (2004), 123–131.

Paavo V Komi and Jukka HT Viitasalo. 1976. Signal characteristics of EMG at different levels of muscle tension. *Acta Physiologica Scandinavica* 96, 2 (1976), 267–276.

Peter Le, Charles A Weisenbach, Emily HL Mills, Lanie Monforton, and Micah J Kinney. 2021. Exploring the interaction between head-supported mass, posture, and visual stress on neck muscle activation. *Human Factors* (2021), 00187208211019154.

Gregory J Lehman and Stuart M McGill. 1999. The importance of normalization in the interpretation of surface electromyography: a proof of principle. *Journal of manipulative and physiological therapeutics* 22, 7 (1999), 444–446.

Wanwan Li, Biao Xie, Yongqi Zhang, Walter Meiss, Haikun Huang, and Lap-Fai Yu. 2020. Exertion-aware path generation. *ACM Trans. Graph.* 39, 4 (2020), 115.

Yilin Liu, Shijia Zhang, and Mahanth Gowda. 2021. NeuroPose: 3D Hand Pose Tracking using EMG Wearables. In *Proceedings of the Web Conference 2021*. 1471–1482.

Jianwen Lou, Yiming Wang, Charles Nduka, Mahyar Hamedi, Ifigeneia Mavridou, Fei-Yue Wang, and Hui Yu. 2019. Realistic facial expression reconstruction for VR HMD users. *IEEE Transactions on Multimedia* 22, 3 (2019), 730–743.

Nancy K Lowe. 1996. The pain and discomfort of labor and birth. *Journal of Obstetric, Gynecologic, & Neonatal Nursing* 25, 1 (1996), 82–92.

Luis R Manssuer, Ralph Pawling, Amy E Hayes, and Steven P Tipper. 2016. The role of emotion in learning trustworthiness from eye-gaze: Evidence from facial electromyography. *Cognitive Neuroscience* 7, 1-4 (2016), 82–102.

Richard W Marklin Jr, Ashley M Toll, Eric H Bauman, John J Simmins, John F LaDisa Jr, and Robert Cooper. 2022. Do Head-Mounted Augmented Reality Devices Affect Muscle Activity and Eye Strain of Utility Workers Who Do Procedural Work? Studies of Operators and Manhole Workers. *Human factors* 64, 2 (2022), 305–323.

Itzel Jared Rodríguez Martínez, Andrea Mannini, Francesco Clemente, and Christian Cipriani. 2020. Online grasp force estimation from the transient EMG. *IEEE Transactions on Neural Systems and Rehabilitation Engineering* 28, 10 (2020), 2333–2341.

Roberto Merletti and Philip J Parker. 2004. *Electromyography: physiology, engineering, and non-invasive applications*. Vol. 11. John Wiley & Sons.

Pedro Monteiro, Guilherme Gonçalves, Hugo Coelho, Miguel Melo, and Maximino Bessa. 2021. Hands-free interaction in immersive virtual reality: A systematic review. *IEEE Transactions on Visualization and Computer Graphics* 27, 5 (2021), 2702–2713.

Inhyuk Moon, Myungjoon Lee, Junuk Chu, and Museong Mun. 2005. Wearable EMG-based HCI for electric-powered wheelchair users with motor disabilities. In *Proceedings of the 2005 IEEE International Conference on Robotics and Automation.* IEEE, 2649–2654.

Masaki Nakada, Tao Zhou, Honglin Chen, Tomer Weiss, and Demetri Terzopoulos. 2018. Deep learning of biomimetic sensorimotor control for biomechanical human animation. *ACM Transactions on Graphics (TOG)* 37, 4 (2018), 1–15.

Nurhazimah Nazmi, Mohd Azizi Abdul Rahman, Shin-Ichiroh Yamamoto, and Siti Anom Ahmad. 2019. Walking gait event detection based on electromyography signals using artificial neural network. *Biomedical Signal Processing and Control* 47 (2019), 334–343.

Yun Suen Pai, Tilman Dingler, and Kai Kunze. 2019. Assessing hands-free interactions for VR using eye gaze and electromyography. *Virtual Reality* 23, 2 (2019), 119–131.

Georgios I Papagiannis, Athanasios I Triantafyllou, Ilias M Roumpelakis, Frantzeska Zampeli, Pinioti Garyfallia Eleni, Panayiotis Koulouvaris, Elias C Papadopoulos, Panayiotis J Papagelopoulos, and George C Babis. 2019. Methodology of surface electromyography in gait analysis: review of the literature. *Journal of medical engineering & technology* 43, 1 (2019), 59–65.

James Paquin and Geoffrey A Power. 2018. History dependence of the EMG-torque relationship. *Journal of Electromyography and Kinesiology* 41 (2018), 109–115.

Sai Akhil Penumudi, Veera Aneesh Kuppam, Jeong Ho Kim, and Jaejin Hwang. 2020. The effects of target location on musculoskeletal load, task performance, and subjective discomfort during virtual reality interactions. *Applied ergonomics* 84 (2020), 103010.

Angkoon Phinyomark and Erik Scheme. 2018. EMG pattern recognition in the era of big data and deep learning. *Big Data and Cognitive Computing* 2, 3 (2018), 21.

Eleana A Pinto, Dimitri ML van Ryckeghem, Ann Meulders, Diana M Torta, Amber Claus, and Stefaan Van Damme. 2021. Motor action changes pain perception: a sensory attenuation paradigm in the context of pain. *Pain* 162, 7 (2021), 2060–2069.

Mamun Bin Ibne Reaz, M Sazzad Hussain, and Faisal Mohd-Yasin. 2006. Techniques of EMG signal analysis: detection, processing, classification and applications. *Biological procedures online* 8, 1 (2006), 11–35.

Simona Rubine-Gatina, Nadina Rimere, Zane Zundane, Alise Gulajeva, and Jelena Reste. 2022. Sternocleidomastoid muscle and head position: How to minimize muscle tension. *IISE Transactions on Occupational Ergonomics and Human Factors* (2022), 1–9.

Nataniel Ruiz, Eunji Chong, and James M Rehg. 2018. Fine-grained head pose estimation without keypoints. In *Proceedings of the IEEE conference on computer vision and pattern recognition workshops.* 2074–2083.

Carolyn M Sommerich, Sharon MB Joines, Veerle Hermans, and Samuel D Moon. 2000. Use of surface electromyography to estimate neck muscle activity. *Journal of Electromyography and kinesiology* 10, 6 (2000), 377–398.

Alexis D Souchet, Domitile Lourdeaux, Alain Pagani, and Lisa Rebenitsch. 2022. A narrative review of immersive virtual reality's ergonomics and risks at the workplace: cybersickness, visual fatigue, muscular fatigue, acute stress, and mental overload. *Virtual Reality* (2022), 1–32.

Tommy Sugiarto, Chun-Lung Hsu, Chi-Tien Sun, Wei-Chun Hsu, Shu-Hao Ye, and Kuan-Ting Lu. 2021. Surface EMG vs. High-Density EMG: Tradeoff Between Performance and Usability for Head Orientation Prediction in VR Application. *IEEE Access* 9 (2021), 45418–45427.

Marcus Thuresson, Björn Äng, Jan Linder, and Karin Harms-Ringdahl. 2005. Mechanical load and EMG activity in the neck induced by different head-worn equipment and neck postures. *International journal of industrial ergonomics* 35, 1 (2005), 13–18.

Marcus Thuresson, Jan Linder, Karin Harms-Ringdahl, et al. 2003. Neck muscle activity in helicopter pilots: effect of position and helmet-mounted equipment. *Aviation, space, and environmental medicine* 74, 5 (2003), 527–532.

Ayumu Tsuboi, Mamoru Hirota, Junki Sato, Masayuki Yokoyama, and Masao Yanagisawa. 2017. A proposal for wearable controller device and finger gesture recognition using surface electromyography. In *SIGGRAPH Asia 2017 Posters.* 1–2.

Anita N Vasavada, Siping Li, and Scott L Delp. 1998. Influence of muscle morphometry and moment arms on the moment-generating capacity of human neck muscles. *Spine* 23, 4 (1998), 412–422.

Andrew D Vigotsky, Israel Halperin, Gregory J Lehman, Gabriel S Trajano, and Taian M Vieira. 2018. Interpreting signal amplitudes in surface electromyography studies in sport and rehabilitation sciences. *Frontiers in physiology* (2018), 985.

Kohei Watanabe and Hiroshi Akima. 2009. Normalized EMG to normalized torque relationship of vastus intermedius muscle during isometric knee extension. *European journal of applied physiology* 106, 5 (2009), 665–673.

Wentao Wei, Qingfeng Dai, Yongkang Wong, Yu Hu, Mohan Kankanhalli, and Weidong Geng. 2019. Surface-electromyography-based gesture recognition by multi-view deep learning. *IEEE Transactions on Biomedical Engineering* 66, 10 (2019), 2964–2973.

Changcheng Wu, Qingqing Cao, Fei Fei, Dehua Yang, Baoguo Xu, Guanglie Zhang, Hong Zeng, and Aiguo Song. 2021. Optimal strategy of sEMG feature and measurement position for grasp force estimation. *PloS one* 16, 3 (2021), e0247883.

Dezhen Xiong, Daohui Zhang, Xingang Zhao, and Yiwen Zhao. 2021. Deep learning for EMG-based human-machine interaction: A review. *IEEE/CAA Journal of Automatica Sinica* 8, 3 (2021), 512–533.

Wolfgang H Zangemeister, Ashby Jones, and Lawrence Stark. 1981. Dynamics of head movement trajectories: main sequence relationship. *Experimental neurology* 71, 1 (1981), 76–91.

Yunxiang Zhang, Benjamin Liang, Boyuan Chen, Paul M Torrens, S Farokh Atashzar, Dahua Lin, and Qi Sun. 2022. Force-aware interface via electromyography for natural VR/AR interaction. *ACM Transactions on Graphics (TOG)* 41, 6 (2022), 1–18.

Yihui Zhao, Zhiqiang Zhang, Zhenhong Li, Zhixin Yang, Abbas A Dehghani-Sanij, and Shengquan Xie. 2020. An EMG-driven musculoskeletal model for estimating continuous wrist motion. *IEEE Transactions on Neural Systems and Rehabilitation Engineering* 28, 12 (2020), 3113–3120.

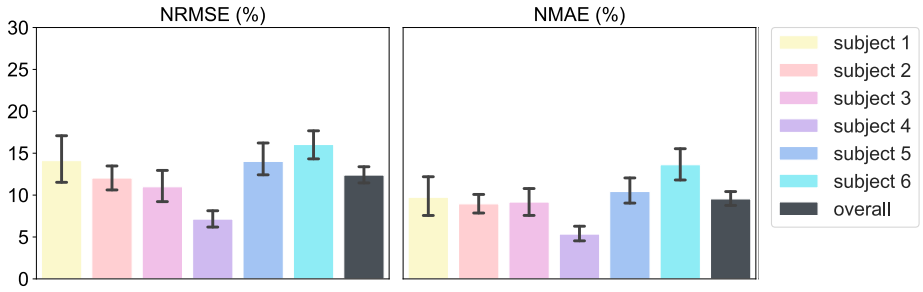

Figure 6: ***Performance of MCLNet for neck MCL estimation when complete head motion trajectories are known.***

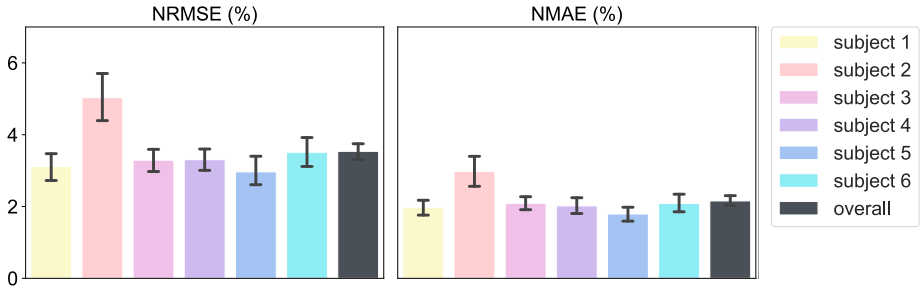

(a) performance of TrajectoryNet for angular velocity prediction (pitch) with target head poses only

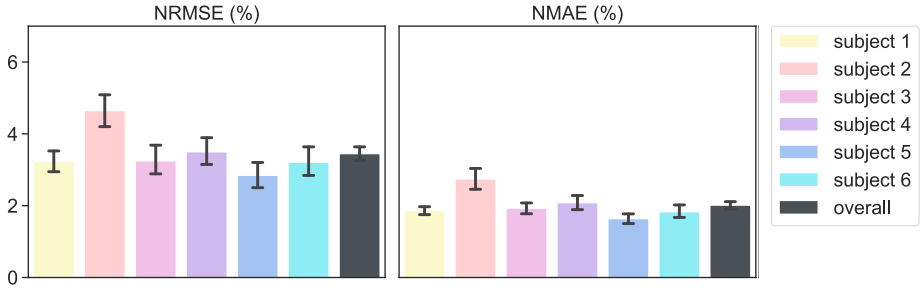

(b) performance of TrajectoryNet for angular velocity prediction (yaw) with target head poses only

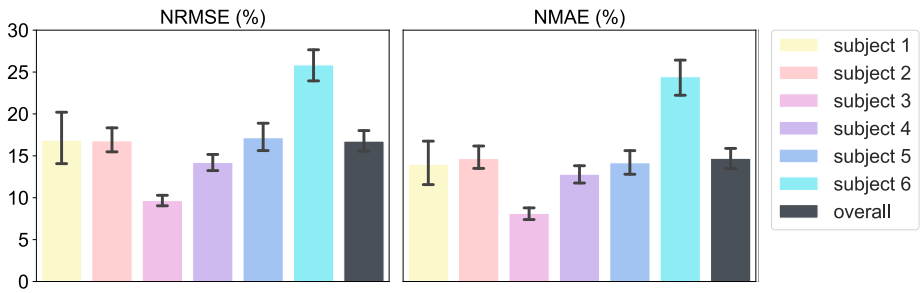

(c) performance of MCLNet coupled with TrajectoryNet for neck MCL prediction with target head poses only

Figure 7: ***Performance of our neck MCL prediction method (MCLNet + TrajectoryNet) with target head poses only.*** **Our method can reliably predict the potential neck MCL of a head movement before it takes place.**

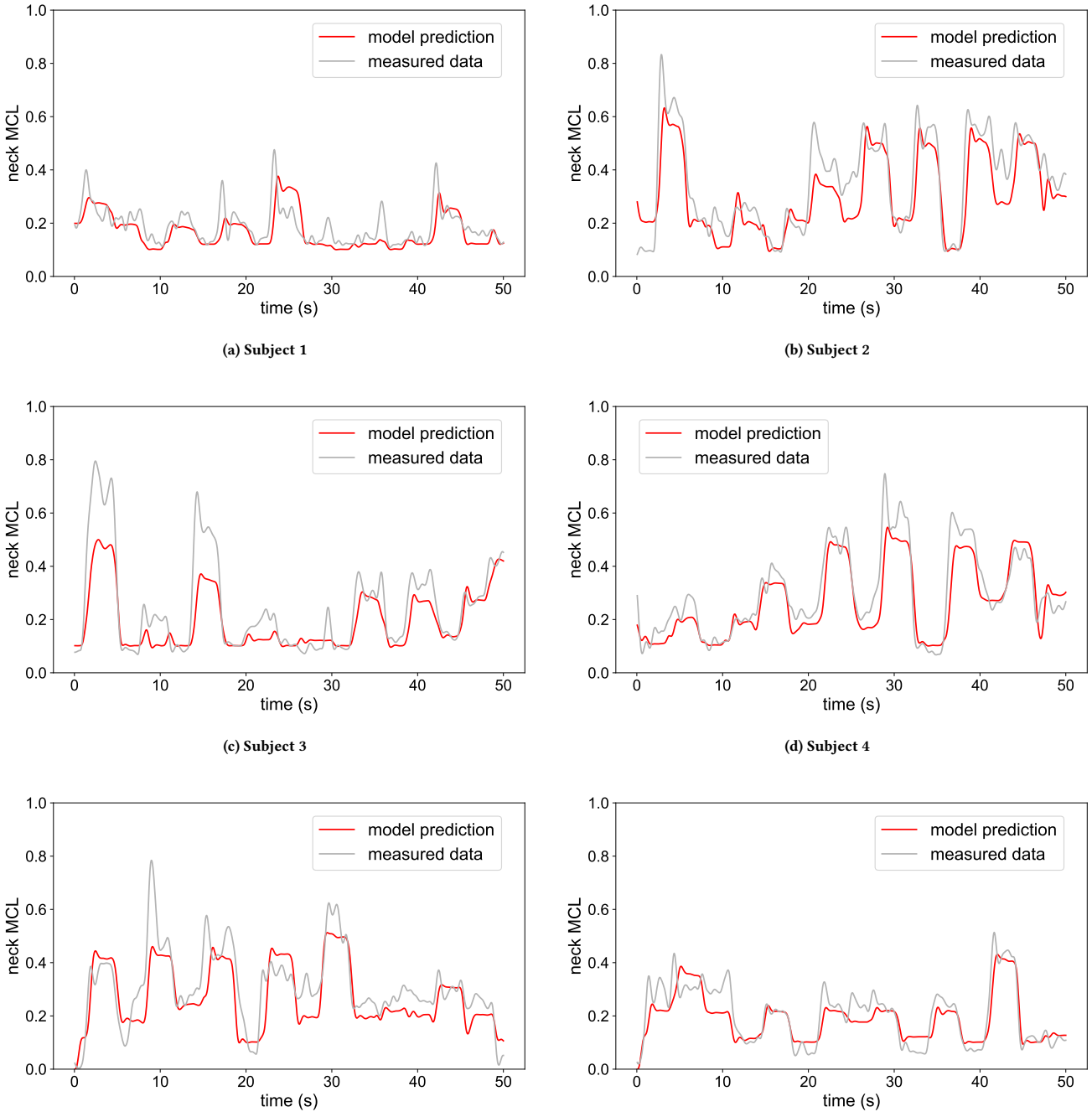

(a) Subject 1

(b) Subject 2

(c) Subject 3

(d) Subject 4

(e) Subject 5

(f) Subject 6

Figure 8: *Qualitative MCL prediction results.* Model-predicted vs. hardware-measured neck MCL for each of the 6 subjects who contributed evaluation data. Each sequence shown is randomly sampled from that particular subject's evaluation data.

A OBTAINING MUSCLE CONTRACTION LEVELS FROM MULTI-CHANNEL RAW EMG SIGNALS

Following standard electromyography (EMG) signal processing approaches [Reaz et al. 2006; Sommerich et al. 2000], we processed and transformed our collected multi-channel raw EMG signals (2D data) into overall neck muscle contraction levels (1D data), or MCL for short. Figure 9 details our EMG data processing pipeline. In addition, each user's total MCL was linearly normalized to $[0, 1]$ to incorporate and mitigate muscular strength/morphology variations across users, such that the MCL values from different users are comparable/consistent and that machine learning on several users' combined data is feasible.

EMG to MCL Data Processing Pipeline

```
function EMG2MCL(EMG)
    ▷ 4-channel EMG signals
    t = GetTimestamps(EMG)        ▷ EMG timestamps
    axis = 0
    bandpass_freq_low = 20 Hz
    bandpass_freq_high = 150 Hz
    lowpass_freq = 1 Hz
    butterworth_order = 4
    ▷ Constant detrending
    EMG = EMG − Mean(EMG, axis)
    ▷ 4th order Butterworth bandpass filter
    sampling_rate = Len(EMG)/(t[−1] − t[0])
    low = (2*bandpass_freq_low)/sampling_rate
    high = (2*bandpass_freq_high)/sampling_rate
    EMG = sos_bp(EMG, order, [low, high], axis)
    ▷ RMS envelope filter
    window = [1/1000, ..., 1/1000]        ▷ 1000-length
    for i ← [0, 4) do:
        EMG[i] = sqrt(conv(EMG[i]^2, window))
    ▷ 4th order Butterworth lowpass filter
    low = (2 * lowpass_freq)/sampling_rate
    EMG = sos_lp(EMG, order, low, axis)
    ▷ Left/Right normalization
    EMG[0] = max(EMG[1])/max(EMG[0])
    EMG[2] = max(EMG[3])/max(EMG[2])
    ▷ Compute overall MCL
    axis = 1
    return sum(EMG, axis)        ▷ Channel-wise sum
end function
```

Figure 9: *Our EMG data processing pipeline.* The illustrated function filters and transforms multi-channel raw EMG signals into overall neck MCL.

B IMPLEMENTATION DETAILS

EMG and head pose data collection and synchronization. To collect EMG signals from both sides of sternocleidomastoid (SCM) and splenius capitis (SC) muscles, we employed 4 Delsys Trigno wireless EMG sensors synchronized at 2000 Hz. The captured 4-channel EMG signals were first wirelessly transmitted to a dedicated EMG base station, which then streamed the data to a Python program running on a desktop PC. To collect head pose data, we took advantage of the high-frequency (90 Hz) head tracking feature on Oculus Quest 2 head-mounted display (HMD). The tracked head pose data were transmitted to a Unity program running on the same desktop PC through Oculus Link. After the EMG data processing procedures described in Supplement A, the two modalities were synchronized using system timestamps and re-sampled to 20 Hz.

Trajectory regression. TrajectoryNet takes in a pair of starting and ending head poses $\{\mathbf{r_s} \in \mathbb{R}^2, \mathbf{r_e} \in \mathbb{R}^2\}$ and outputs the parameters of predicted Gaussian-shaped angular velocity curves for both pitch and yaw directions $\{A^i, \mu^i, \sigma^i\}_{i\in\{p,y\}}$. Specifically, $\{\mathbf{r_s}, \mathbf{r_e}\}$ are first transformed into $\{\mathbf{r_s}, \mathbf{r_e} - \mathbf{r_s}\}$ and then concatenated into a vector of length 4 before feeding into TrajectoryNet for accelerated convergence during training and improved generalization ability of the model. To obtain the head motion trajectory $\mathbf{r}_t(\mathbf{r_s}, \mathbf{r_e})$ associated with the predicted angular velocity $\boldsymbol{\omega}_t(\mathbf{r_s}, \mathbf{r_e})$, we integrate it over $[t_s = 0, t_e]$, where t_e is determined such that:

$$\mathbf{r_s} + \int_{t=0}^{t_e} \boldsymbol{\omega}_t(\mathbf{r_s}, \mathbf{r_e})\mathrm{d}t = \mathbf{r_e}. \tag{7}$$

MCL estimation. The inputs to our MCLNet are composed of a head motion sequence of T=400ms, which is equivalent to 8 samples of pitch/yaw angles under the re-sampling rate of 20 Hz, and the corresponding angular acceleration values computed via finite difference (8 samples of pitch/yaw angular acceleration). Given the pair of input head motion and angular acceleration sequences (T=400ms, 8 samples for each), MCLNet outputs the instantaneous MCL for the central 200ms interval (4 samples under the sampling rate of 20 Hz), i.e., compared to the outputs, the inputs cover additional 100ms in both directions of the time axis.

TrajectoryNet and MCLNet architectures. TrajectoryNet consists of 3 repeating FullyConnected-BatchNorm1D-ReLU blocks (the number of channels was set to 20, and the last block does not contain BatchNorm1D layer). The passive torque module $\mathcal{T}_\mathbf{p}(\cdot)$ and torque-to-MCL module $\mathcal{E}(\cdot)$ of MCLNet were approximated by two 1D convolutional neural network (CNN) models. Specifically, $\mathcal{T}_\mathbf{p}(\cdot)$ consists of 3 repeating Convolution1D-BatchNorm1D-ReLU blocks (number of channels was set to 20, and the last block does not contain ReLU activation); $\mathcal{E}(\cdot)$ consists of 3 repeating Convolution1D-BatchNorm1D-ReLU blocks (number of channels was set to 20), with the second one followed by a 1D MaxPooling layer (both kernel size and stride were set to 2) and the last one followed by a 20×1 FullyConnected layer.

TrajectoryNet and MCLNet training. TrajectoryNet was optimized using L_2 loss and Adam optimizer ($\beta_1 = 0.9, \beta 2 = 0.999$) for 25 epochs. The learning rate started at $1e^{-3}$ and dropped by 10× at epoch 15. The batch size was set to 64. A weight decay factor of $1e^{-5}$ was enforced to reduce over-fitting. MCLNet was optimized using L_2 loss and Adam optimizer ($\beta_1 = 0.9, \beta 2 = 0.999$) for 20 epochs. The learning rate started at $1e^{-3}$ and dropped by 10× at

epoch 10. The batch size was set to 64. A weight decay factor of $5e^{-4}$ was enforced to reduce over-fitting.

C HEAD MOTION STATISTICS

During both the pilot study (Section 3) and psychophysical study (Section 5.3), participants were instructed to move their heads as naturally as possible. No instruction or control on their head motion speed was given and participants were free to move faster or slower as they felt necessary. In our dataset, the maximum and mean velocities (degrees per second) for pitch/yaw are 182/238 and 94/133, while the maximum and mean accelerations (degrees per second squared) are 388/507 and 179/287.

D GENERATING USER STUDY CONDITIONS

Figure 10 provides the implementation details of the condition generation algorithm in our psychophysical user study (Section 5.3).

User Study Condition Generation

```
function GetNextPose(r_s, t, θ°, Condition)
    ▷ Unif. sample 180 head poses that are θ° from r_s
    poses = UniformSample(r_s, θ°, 180)
    all_traj = []
    for r_e ← poses do:
        ▷ Predict the head trajectory from r_s to r_e
        trajectory = TrajectoryNet(r_s, r_e)
        ▷ Include 1-second fixation on r_e
        trajectory = AddFixation(trajectory, r_e)
        all_traj.Append(trajectory)
    ▷ Pick candidate with highest score as next pose
    maxScore = −Inf
    Init r                ▷ Current candidate for next pose
    for i ← [0, ..., len(all_traj)-1] do:
        r_e = GetEndPose(all_traj[i])
        if Condition == MAX:
            score = C(r_{j∈[1,t]}, r_e) + H_c(all_traj[i])
        if Condition == RND:
            score = C(r_{j∈[1,t]}, r_e)
        if Condition == MIN:
            score = C(r_{j∈[1,t]}, r_e) − H_c(all_traj[i])
        ▷ Update r if score greater than maxScore
        if score > maxScore:
            maxScore = Score
            r = r_e
    return r
end function
```

Figure 10: *User study condition generation algorithm.* Given the current head pose r_e on a scan path, this function extends the scan path by generating the optimal next head pose r for one of the 3 conditions MAX/MIN/RND.

E INDIVIDUAL VOTES IN USER STUDY

Table 1 summarizes all 12 user study (Section 5.3) participants' two-alternative forced choice (2AFC) response distribution across the three conditions: **MAX**, **RND**, and **MIN**. Each number indicates the number of times that a particular condition was chosen as the more uncomfortable one over all 18 2AFC sessions.

cond \ user	#1	#2	#3	#4	#5	#6	#7	#8	#9	#10	#11	#12
MAX	11	12	11	12	10	10	9	12	9	10	9	9
RND	5	5	6	4	4	7	8	6	7	6	6	9
MIN	2	1	1	2	4	1	1	0	2	2	3	0

Table 1: *Individual 2AFC results in user study.* The numbers indicate, for each participant and each condition, how many trials among all 18 2AFC sessions that particular condition was rated by that particular participant as being more uncomfortable.